Surface collective oscillations of metal clusters and spheres: Random-phase-approximation sum-rules approach

Ll. Serra, F. Garcias, and M. Barranco
Departament de Física, Universitat de les Illes Balears, E-07071 Palma de Mallorca, Spain

J. Navarro
Departament de Física Atòmica, Molecular i Nuclear y Instituto de Física Corpuscular, Universitat de València, Burjassot, València, Spain

C. Balbás and A. Mañanes
Departamento de Física Teórica, Atómica y Nuclear, Universidad de Valladolid, E-47011 Valladolid, Spain
(Received 28 November 1988)

Using the once and thrice energy-weighted moments of the random-phase-approximation strength function, we have derived compact expressions for the average energy of surface collective oscillations of clusters and spheres of metal atoms. The $L=0$ volume mode has also been studied. We have carried out quantal and semiclassical calculations for Na and Ag systems in the spherical-jellium approximation. We present a rather thorough discussion of surface diffuseness and quantal size effects on the resonance energies.

I. INTRODUCTION

The study of surface modes of metal spheres has drawn some attention in the past[1-3] and is the subject of a renewed interest.[4-7] Very recently, some experimental information on surface modes[8,9] and electric polarizabilities[10] of similar systems, namely metal clusters, has been obtained. It seems that the gross features of the experimental findings are well reproduced by a self-consistent time-dependent local-density approximation (TDLDA), in which the small metal particles are modeled by a self-consistent spherical-jellium model.[11-13]

Unfortunately, these TDLDA calculations require a substantial numerical effort that is very likely quite formidable. Moreover, some of the physics might be obscured by the unavoidable numerical apparatus. These facts prompted Bertsch and Ekardt[14] to use in this context the random-phase-approximation (RPA) sum-rule approach, which has proven to be extremely useful in describing giant resonances in atomic nuclei.[15,16] It is worth emphasizing that RPA is the small-amplitude limit of TDLDA and, consequently, both methods are completely equivalent for studying the energy spectrum of these systems.

The purpose of the present work is to extend that of Ref. 14 to all multipole surface modes, and also to present some results for the $L=0$ volume mode. We will rely heavily on similar work recently done on isoscalar nuclear giant resonances.[17-19]

The basic hypotheses of our model are the following.

(i) The mean field created by the positive ions is obtained in the spherical-jellium approximation.

(ii) The valence electrons are described in a local-density approximation (LDA), either by a Kohn-Sham (KS) or by a Thomas-Fermi (TF) method. Of course, the RPA sum rules will be deduced in the KS framework.

(iii) The external field acts only on the valence electrons.

These hypotheses are currently used in microscopic calculations of metal spheres and metal clusters.[11-13] Thus, the method we use in this work applies to both systems.

This paper is organized as follows. We shall describe the RPA sum rules in Sec. II. The KS and TF models we have used will be briefly discussed in Sec. III. The numerical results for the surface modes and the $L=0$ volume mode will be presented in Sec. IV. Finally, we shall make some concluding remarks in Sec. V.

II. RPA SUM RULES

A. General description

RPA sum rules are described in great detail in Refs. 15 and 16. We refer the interested reader to these references where, besides a clear exposure of the fundamental results, one may find references to earlier work in this field.

Sum rules m_k are moments of the strength function

$$S(E)=\sum_n \delta(E-E_n)|\langle n|Q|\phi\rangle|^2 , \quad (1)$$

where the sum (integral in the case of continuum spectrum) extends over all the excited states of the system. Q is the external field acting on the system; E_n, $|n\rangle$, and $|\phi\rangle$ are the excitation energies, the excited states and the ground state (g.s.) of the system, respectively. The moment of order k is defined as

$$m_k=\int E^k S(E)dE=\sum_n E_n^k|\langle n|Q|\phi\rangle|^2 . \quad (2)$$

From these moments, the average energy and variance of

 ©1989 The American Physical Society

the strength can be obtained:

$$\bar{E}=\frac{m_1}{m_0}\ ,$$
$$\sigma^2=\frac{m_2}{m_0}-\frac{m_1^2}{m_0^2}\ . \tag{3}$$

Obviously, a direct computation of m_k from Eq. (2) is hopeless in most practical cases because one should know the whole spectrum. However, *odd* moments of $S(E)$ can be obtained with RPA precision as expectation values on the KS *ground state* $|\phi\rangle$ of suitable operators.

Defining $E_k \equiv (m_k/m_{k-2})^{1/2}$, it has been shown that[15]

$$E_1 \le \bar{E} \le E_3\ ,$$
$$\sigma^2 \le \tfrac{1}{4}(E_3^2-E_1^2)\ . \tag{4}$$

Consequently, one may estimate the centroid and variance of the strength function by evaluating the three RPA moments m_{-1}, m_1, and m_3. If most of the strength is in a narrow energy region, as it is in the case of some resonance states, then E_1 and E_3 are estimates of the mean resonance energy. Conversely, if E_1 and E_3 are close, we deduce that some strength is concentrated around these values. For m_1 and m_3 we have

$$m_1=\tfrac{1}{2}\langle\phi|[Q,[H,Q]]|\phi\rangle\ ,$$
$$m_3=\tfrac{1}{2}\langle\phi|[[H,[H,Q]],[H,Q]]|\phi\rangle\ . \tag{5}$$

The double commutator entering the definition of m_1 is easy to evaluate when Q only depends on the position. This is not quite so for m_3, which is more easy to obtain by scaling the Slater determinant $|\phi\rangle$. Indeed, defining the scaled wave function

$$|\phi_\eta\rangle \equiv e^{\eta[H,Q]}|\phi\rangle\ , \tag{6}$$

we get

$$m_3=\frac{1}{2}\frac{\partial^2}{\partial\eta^2}\langle\phi_\eta|H|\phi_\eta\rangle\Big|_{\eta=0}\ . \tag{7}$$

If $[H,Q]$ is a one-body operator, $|\phi_\eta\rangle$ is still a determinantal wave function (w.f.) and m_3 is obtained with RPA precision. Let us define the scaled particle and kinetic-energy densities:

$$\rho_\eta(\vec{r})\equiv\langle\phi_\eta|\hat{\rho}|\phi_\eta\rangle=\rho+\eta\rho_1+\eta^2\rho_2+\cdots\ ,$$
$$\tau_\eta(\vec{r})\equiv\langle\phi_\eta|\hat{\tau}|\phi_\eta\rangle=\tau+\eta\tau_1+\eta^2\tau_2+\cdots\ , \tag{8}$$

where

$$\hat{\rho}=\sum_i \delta(\vec{r}-\vec{r}_i)\ ,$$
$$\hat{\tau}=\sum_i \overleftarrow{\nabla}_i\delta(\vec{r}-\vec{r}_i)\vec{\nabla}_i\ , \tag{9}$$

and

$$\rho=\langle\phi|\hat{\rho}|\phi\rangle\ ,$$
$$\rho_1=\langle\phi|[\hat{\rho},[H,Q]]|\phi\rangle\ ,$$
$$\rho_2=\tfrac{1}{2}\langle\phi|[[\hat{\rho},[H,Q]],[H,Q]]|\phi\rangle\ , \tag{10}$$

with similar expressions for τ, τ_1, and τ_2. Developing the expectation value (7) in powers of η, the above expressions allow for a straightforward (but usually cumbersome) evaluation of m_3.

B. The sum rules m_1 and m_3 for $Q=r^L Y_{L0}$

This field generates surface oscillations. Indeed, for a velocity-independent potential, it is easy to prove that the transition density ρ_1 reads

$$\rho_1=-\hbar\vec{\nabla}[\rho\vec{u}]\ , \tag{11}$$

where $\vec{u}$ is the collective velocity

$$\vec{u}=\frac{\hbar}{m}\vec{\nabla}Q\ , \tag{12}$$

and ρ is the *g.s. equilibrium density*. Equation (12) shows that the velocity field is irrotational. Since $\Delta Q=0$, we have

$$\rho_1=-\frac{\hbar^2}{m}\vec{\nabla}\rho\cdot\vec{\nabla}Q\ , \tag{13}$$

which is peaked at the surface. The general expression for ρ_2 is

$$\rho_2=\tfrac{1}{2}\hbar^2\vec{\nabla}[\vec{u}\cdot\vec{\nabla}(\rho\vec{u})]=-\tfrac{1}{2}\hbar[\vec{u}\cdot\vec{\nabla}+(\vec{\nabla}\cdot\vec{u})]\rho_1\ , \tag{14}$$

which in the present case becomes

$$\rho_2=-\frac{\hbar^2}{2m}\vec{\nabla}Q\cdot\vec{\nabla}\rho_1\ . \tag{15}$$

Equations (13) and (15) explicitly show that $\int\rho_i d\vec{r}=0$, $i=1,2$. It is worth noting that the condition $\mathrm{div}\vec{u}=0$ is the origin of the surface character of the oscillations generated by Q. That will be more clear when we discuss the $L=0$ case.

A direct evaluation of m_1 yields[19]

$$m_1=\frac{\hbar^2}{2m}L(2L+1)\int_0^\infty dr\, r^{2L}\rho(r)\ , \tag{16}$$

where $\rho(r)$ is the KS g.s. equilibrium density. For $L=1$, it is proportional to the electron number N:

$$m_1(L=1)=\frac{\hbar^2}{2m}\frac{3N}{4\pi}\ , \tag{17}$$

and for $L=2$, proportional to the square of the (rms) radius

$$m_1(L=2)=\frac{\hbar^2}{2m}\frac{10N}{4\pi}\langle r^2\rangle\ ,$$
$$\langle r^2\rangle\equiv\frac{1}{N}\int d\vec{r}\,r^2\rho(r)\ . \tag{18}$$

The m_3 sum rule will consist of three terms, one $[m_3(T)]$ coming from the kinetic-energy density in H and two from the electron-electron Coulomb energy

$[m_3(e\text{-}e)]$ and the jellium-electron Coulomb energy $[m_3(j\text{-}e)]$. Altogether, both Coulomb contributions will be referred to as $m_3(C)$. It has been proven[19] that pure volume terms, i.e., terms that only depend on the electron density, like the Coulomb-exchange contribution in the Slater approximation or the correlation energy in the Lang-Kohn approximation,[20] *do not contribute* to m_3. That can be easily seen using the technique we will outline below to obtain $m_3(e\text{-}e)$ and $m_3(j\text{-}e)$.

The term $m_3(T)$ can be written as[19]

$$m_3(T)=\left[\frac{\hbar^2}{m}\right]^2 L(2L+1)(L-1) \times\int_0^\infty dr\,\frac{\hbar^2}{2m}r^{2L-2}[L\tau+\tfrac{1}{2}(L-2)\lambda]\ . \quad (19)$$

The function λ reads

$$\lambda(r)=\frac{1}{4\pi r^2}\sum_\alpha 2(2L_\alpha+1)L_\alpha(L_\alpha+1)\frac{|u_\alpha(r)|^2}{r^2}\ , \quad (20)$$

where $u_\alpha(r)/r$ is the radial single-electron wave function. $\lambda(r)$ represents a centrifugal kinetic-energy density, and in the $\hbar^0$-order TF approximation one has $\lambda=2\tau/3$.

Let us work out in some detail the Coulomb contributions.[21] From Eqs. (7), (8), and (10) the electron-electron part can be written as

$$m_3(e\text{-}e)=\frac{1}{2}\frac{\partial^2}{\partial\eta^2}E(e\text{-}e)\Big|_{\eta=0} =\tfrac{1}{2}e^2\left[\int\int\frac{\rho_1(\vec{r}_1)\rho_1(\vec{r}_2)}{|\vec{r}_1-\vec{r}_2|}d\vec{r}_1\,d\vec{r}_2 +2\int\int\frac{\rho(\vec{r}_1)\rho_2(\vec{r}_2)}{|\vec{r}_1-\vec{r}_2|}d\vec{r}_1\,d\vec{r}_2\right]\ . \quad (21)$$

Using the multipole expansion of $|\vec{r}_1-\vec{r}_2|^{-1}$, the first integral in Eq. (21) reduces to

$$\int\int\frac{\rho_1(\vec{r}_1)\rho_1(\vec{r}_2)}{|\vec{r}_1-\vec{r}_2|}d\vec{r}_1\,d\vec{r}_2=\left[\frac{\hbar^2}{m}\right]^2 L^2\int d\vec{r}\,\rho^2 r^{2L-2}\ , \quad (22)$$

while the second integral reads

$$2\int\int\frac{\rho(\vec{r}_1)\rho_2(\vec{r}_2)}{|\vec{r}_1-\vec{r}_2|}d\vec{r}_1\,d\vec{r}_2 =2\int d\mathbf{r}_1\rho(\mathbf{r}_1)\int_0^\infty dr_2 r_2^2\frac{1}{r_>}\int d\Omega_2\rho_2(\mathbf{r}_2)\ . \quad (23)$$

The integral over the angles yields

$$\int\rho_2(\vec{r}_2)d\Omega_2=\frac{1}{2}\left[\frac{\hbar^2}{m}\right]^2 L^2 r_2^{L-1} \times\left[\frac{d}{dr_2}+\frac{L+1}{r_2}\right]\left[\rho'(r_2)r_2^{L-1}\right]\ . \quad (24)$$

Thus Eq. (23) reduces to

$$4\pi L^2\left[\frac{\hbar^2}{m}\right]^2\int_0^\infty dr_2\,r_2^{2L-2}\rho'(r_2)\int_0^{r_2}dr_1\,r_1^2\rho(r_1)\ . \quad (25)$$

Finally, integrating Eq. (25) by parts and adding it to Eq. (22) yields

$$m_3(e\text{-}e)=-e^2\left[\frac{\hbar^2}{m}\right]^2 L^2(L-1) \times\int_0^\infty dr_2\,\rho(r_2)r_2^{2L-3}\int_0^{r_2}d\vec{r}_1\rho(r_1)\ , \quad (26)$$

as was first shown in Ref. 19. Similarly, the jellium-electron term reads

$$m_3(j\text{-}e)=-e^2\int\int\frac{\rho_j(r_1)\rho_2(\vec{r}_2)}{|\vec{r}_1-\vec{r}_2|}d\vec{r}_1\,d\vec{r}_2\ , \quad (27)$$

where $\rho_j(r_1)$ is the jellium density, a step function in our case. Equation (27) is analogous to Eq. (23) if we identify $\rho_j(r_1)$ and $\rho(r_1)$. Consequently, $m_3(j\text{-}e)$ is given by

$$m_3(j\text{-}e)=-2\pi e^2L^2\left[\frac{\hbar^2}{m}\right]^2 \times\int_0^\infty dr_2\,r_2^{2L-2}\rho'(r_2)\int_0^{r_2}dr_1\,r_1^2\rho_j(r_1)\ , \quad (28)$$

where $\rho'(r_2)$ is the density derivative with respect to r. Equations (19), (26), and (28) are the sought-after expressions for m_3. Together with m_1, Eq. (16), they will be used in Sec. IV to obtain estimates of the resonance energies.

It is worth mentioning that in the dipole case, only $m_3(j\text{-}e)$ contributes to the "restoring force" represented by m_3. Indeed, the electron-electron kinetic and Coulomb contributions vanish because the operator rY_{10} corresponds to a translation of the electron cloud as a whole. Only the translational symmetry-breaking jellium field gives a nonzero contribution.

C. The sum rules m_1, m_3, and m_{-1} for $Q=r^2$

This field will generate monopole volume oscillations. It has been thoroughly studied in the nuclear case.[15] It is easy to show that

$$m_1=2\frac{\hbar^2}{m}N\langle r^2\rangle\ . \quad (29)$$

The scaling (6) of the electron wave functions is particularly simple for $Q=r^2$. Defining

$$\alpha=\exp\left[\frac{-2\hbar^2\eta}{m}\right]\ ,$$

we get

$$m_3=\frac{1}{2}\left[\frac{2\hbar^2}{m}\right]^2\frac{\partial^2E}{\partial\alpha^2}\Big|_{\alpha=1}\ . \quad (30)$$

The scaling of the w.f. induces the following scaling on the particle and kinetic-energy densities:

$$\rho(r)\rightarrow\rho_\alpha(r)=\alpha^3\rho(\alpha r)\ ,$$
$$\tau(r)\rightarrow\tau_\alpha(r)=\alpha^5\tau(\alpha r)\ . \tag{31}$$

Developing $\rho_\alpha(r)$ around $\alpha=1$ we have

$$\rho_\alpha(r)=\rho_{\alpha=1}(r)+\rho'_{\alpha=1}(r)(\alpha-1)+\tfrac{1}{2}\rho''_{\alpha=1}(r)(\alpha-1)^2+\cdots\ ,$$

where $\rho_{\alpha=1}(r)$ is the ground-state equilibrium density,

$$\rho'_{\alpha=1}(r)=\rho_1=3\rho(r)+r\rho'(r)=3\rho(r)+\vec{r}\cdot\vec{\nabla}\rho(r)\ ,$$
$$\tfrac{1}{2}\rho''_{\alpha=1}(r)=\rho_2=\tfrac{1}{2}(6\rho+4\vec{r}\cdot\vec{\nabla}\rho+r^2\,\Delta\rho)\ . \tag{32}$$

It is easy to check that $\int\rho_i\,d\vec{r}=0$, $i=1,2$. Notice that for $L=0$ the transition density ρ_1 is not peaked at the surface, having a node at the value of r such that $3\rho(r)+r\rho'(r)$ is equal to zero.

For an electron functional consisting of a kinetic term (T), a direct Coulomb term (E_c), a Coulomb exchange term of Slater type (E_{Cx}), and a correlation term of Lang-Kohn type,[20]

$$E_{\rm corr}=-a\int\frac{\rho}{b+(3/4\pi\rho)^{1/3}}d\vec{r}\ , \tag{33}$$

plus a jellium-jellium term ($E_{j\text{-}j}$) and a jellium-electron term,

$$E_{j\text{-}e}=\int V_j(r)\rho(r)d\vec{r}\ , \tag{34}$$

where V_j is the jellium Coulomb potential, the scaling of the total energy yields

$$E(\alpha)=\alpha^2T+\alpha E_{Cx}+\alpha E_C+\int V_j\alpha^3\rho(\alpha r)d\vec{r}-a\int\frac{\rho}{b+(1/\alpha)(3/4\pi\rho)^{1/3}}d\vec{r}\ . \tag{35}$$

Thus

$$m_3=\frac{1}{2}\left[\frac{2\hbar^2}{m}\right]^2\left[2T+\int V_j(6\rho+4r\rho'+r^2\,\Delta\rho)d\vec{r}+a\int\frac{2b(4\pi/3)^{2/3}\rho^{5/3}}{[b(4\pi\rho/3)^{1/3}+1]^3}d\vec{r}\right]\ . \tag{36}$$

Again, the calculation of m_3 only involves g.s. quantities, like the kinetic energy T or the electron density ρ. This is one of the merits of this approach.

Generally speaking, the volume terms do contribute to m_3 for volume modes. However, notice that for $Q=r^2$ the electron-electron Coulomb energy contributes to m_3 through self-consistency, but not explicitly because it scales linearly with α. We anticipate that the correlation-energy contribution to m_3 is very small.

The m_{-1} sum rule, which is closely related to the polarizability of the system, can be obtained by solving the constrained Hamiltonian $H+\lambda Q$. It can be shown[15] that

$$m_{-1}=\sum_n\frac{1}{E_n}|\langle n|Q|\phi\rangle|^2=-\frac{1}{2}\frac{d\langle Q_\lambda\rangle}{d\lambda}\bigg|_{\lambda=0}\ . \tag{37}$$

This is easy to evaluate only in the monopole case $Q=r^2$ because it is spherically symmetric. Since we are mainly interested in surface modes, we shall leave the calculation of the polarizabilities for a forthcoming study, except for this $L=0$ mode.

III. THE KOHN-SHAM AND THOMAS-FERMI MODELS

We have seen in the preceding section that to evaluate the RPA sum rules one needs to solve the g.s. KS equations. In the context of metal clusters, this has been done some time ago (see, for example, Refs. 22 and 23). The corresponding TF (or density-functional formalism) equations have also been solved (see, for example, Ref. 24). Consequently, we shall present here the main formulas and results just for the sake of completeness and further reference. In this section, we use atomic units throughout, i.e., energies are in units of 2 Ry=27.2 eV, and lengths in units of the Bohr radius $a_0=0.529$ Å.

We shall apply the method described in the preceding section to Na and Ag systems. The radius of the jellium sphere is $R=r_sN^{1/3}$, where N is the number of atoms and r_s the ionic radius. We have taken $r_s=4.0$ a.u. for Na and 3.0 a.u. for Ag and have used the following LDA functional:

$$E[\rho]=T-\frac{3}{4}\left[\frac{3}{\pi}\right]^{1/3}\int\rho^{4/3}d\vec{r}-\int\frac{0.44\rho}{7.8+(3/4\pi\rho)^{1/3}}d\vec{r}+\tfrac{1}{2}\int\int\frac{\rho(r)\rho(r')}{|\vec{r}-\vec{r}'|}d\vec{r}\,d\vec{r}'+\int V_j(r)\rho(r)d\vec{r}+E_{j\text{-}j}\ , \tag{38}$$

TABLE I. Total energies E and rms radii $\langle r^2\rangle^{1/2}$ of some magic Na clusters in the KS and TF approximations, in the latter case for two different values of the von Weizsäcker coefficient β [Eq. (40)].

	KS		TF($\beta=1$)		TF($\beta=0.65$)	
N	E	$\langle r^2\rangle^{1/2}$	E	$\langle r^2\rangle^{1/2}$	E	$\langle r^2\rangle^{1/2}$
8	−0.580	6.64	−0.380	6.97	−0.453	6.77
20	−1.49	8.76	−1.15	8.93	−1.28	8.80
40	−3.02	10.88	−2.53	10.98	−2.73	10.89
58	−4.46	12.21	−3.81	12.33	−4.06	12.25
92	−7.16	14.18	−6.27	14.27	−6.61	14.20
138	−10.81	16.18	−9.68	16.25	−10.12	16.20
198	−15.53	18.26	−14.17	18.27	−14.73	18.22

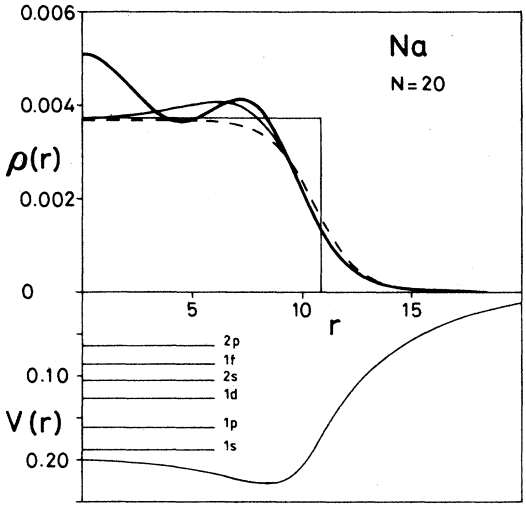

FIG. 1. Densities $\rho(r)$ and single-electron potential $V(r)$ (in a.u.) corresponding to the $N=20$ Na cluster. The thick line is the KS density, whereas the thin one is the variational TF density. Also displayed are the adjusted TF density (dashed line) and the constant jellium density. The horizontal lines represent some of the single-electron levels. Starting from the bottom, they correspond to the $1s$, $1p$, $1d$, $2s$, $1f$, and $2p$ states.

where $E_{j\text{-}j}$ is the jellium Coulomb energy and T the electron kinetic energy:

$$T=\tfrac{1}{2}\int d\vec{r}\,\tau(r)\ ,$$

with

$$\tau(r)=\sum_i |\vec{\nabla}\varphi_i|^2 \tag{39}$$

in the KS approximation and

$$\tau(r)=\tfrac{3}{5}(3\pi^2)^{2/3}\rho^{5/3}+(\beta/4)(\vec{\nabla}\rho)^2/\rho \tag{40}$$

in the TF approximation. The effective parameter β that multiplies the von Weizsäcker correction to the $\rho^{5/3}$ term

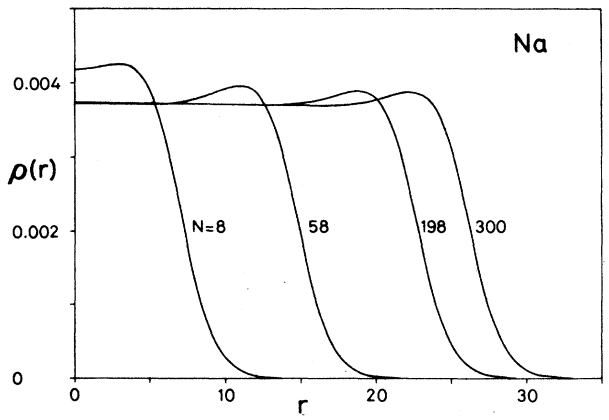

FIG. 2. TF densities of some Na clusters. From inside outwards, they correspond to $N=8$, 58, 198, and 300.

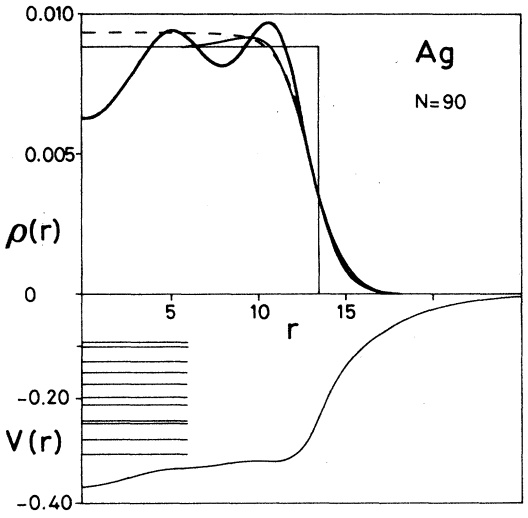

FIG. 3. Same as Fig. 1 for the $N=90$ Ag cluster. Starting from the bottom, the single-electron levels correspond to $1s$, $1p$, $1d$, $2s$, $1f$, $2p$, $1g$, $2d$, $1h$, $2f$, and $3p$ states.

has been adjusted to reproduce the KS results on average. Indeed, β has a big influence on the electron surface diffuseness and on the exponential falloff of the electron density as well. Usally, a value of $\beta=1$ is taken.[21,24] Here we have employed $\beta=0.65$ for these two metals, although a slightly smaller value would have yielded better results in the case of Ag. To give an idea of how TF($\beta=1$) and TF($\beta=0.65$) compare with KS, we have collected in Table I the total energies and rms radii (in atomic units) of some magic Na clusters.

Figure 1 shows the densities corresponding to the $N=20$ Na cluster, the KS single-particle potential $V(r)$, and the electron single-particle levels, the upper two being empty. The thick solid line is the KS density, whereas the thin solid line is the variational TF density. Also shown is the jellium constant density.

We have adjusted the variational TF densities to a two-parameter Fermi function:

$$\rho=\frac{\rho_0}{1+\exp[(r-R)/a]^\nu}\ , \tag{41}$$

taking $\nu=1$. For Na clusters, the average values $R=r_0N^{1/3}$ with $r_0=3.9$ a.u. (slightly smaller than the ionic radius r_s) and $a=1.02$ a.u. reproduce fairly well the variational TF densities for $N\geq 20$ clusters. We have also let free the parameter ν and found that $\nu\approx 1$. The dashed line in Fig. 1 is the adjusted density, Eq. (41). The agreement between variational and adjusted TF densities is much better for bigger clusters.

Figure 2 displays the variational TF electron densities of the $N=8$, 58, 198, and 300 Na clusters. The central densities tend to $\rho_0=3.73\times 10^{-3}$ a.u., which is the bulk value $3/4\pi r_s^3$.

Figure 3 shows the magic $N=90$ Ag cluster using the same convention as in Fig. 1. Since the Ag ionic radius is smaller than the Na radius, the clusters are more com-

pact for the former than for the latter. For silver, the two-parameter Fermi functions that better adjust the variational TF densities have $r_0=2.9$ and $a=0.92$ a.u. We have found that $N=8$, 20, 40, 58, and 90 Ag clusters are "magic," whereas, for Na, 92 is magic instead of 90. Starting from the bottom, the single-particle electron levels for $N=90$ Ag are $1s$, $1p$, $1d$, $2s$, $1f$, $2p$, $1g$, $2d$, $1h$, $2f$, and $3p$, the last two being empty. The $3s$ state, which is next to $1h$ in $N=90$ Na, lies at $\epsilon(3s)\approx -0.046$ a.u. in the case of Ag.

To conclude this section we would like to say a word of caution about using sum rules in conjunction with the TF method. The deduction of m_1 and m_3 explicitly uses the KS electron wave functions; only in the case in which we use them to build the g.s. Slater determinant $|\phi\rangle$, Eqs. (4) will give us the RPA m_1 and m_3 moments. As an example of the danger of *first* using a TF LDA approximation and then scaling the electron density according to the first of Eqs. (8), notice that if we had proceeded this way, the *leading* term of the kinetic-energy density, which is proportional to $\rho^{5/3}$, *would not have contributed* to $m_3(T)$ for $L>1$ because it is a pure volume term. However, if one uses a semiclassical model for ρ and τ *after* arriving at the RPA expressions for m_1 and m_3, one may expect to obtain a fair estimate of the true RPA moments. That was the point of view of Refs. 17 and 18, which we shall also adopt here when we present the TF results.

IV. NUMERICAL RESULTS

Table II collects the $L=0$ results corresponding to three magic Na clusters, $N=8$, 20, and 92 (the numerical results presented in this section are in atomic units). Notice first that E_1 and E_3 are rather close, indicating that some monopole strength is concentrated in this energy region. A similar concentration was found by Bertsch and Ekardt for the $L=1$ surface mode.[14] This table also shows that the main contribution to $m_3(L=0)$ comes from $m_3(j\text{-}e)$. $m_3(T)$ and m_3(corr) [last term in Eq. (36)] contribute very little, altogether $\approx 12\%$ for $N=8$ and $\approx 1\%$ for a cluster of 198 Na atoms.[21]

Tables III–V show the surface-mode results corresponding to the same clusters for several values of L. E_3 decreases at very high values of L (see especially Table III). This is due to the finite potential well at which electrons are submitted, as is discussed in Ref. 25. It is quite interesting to observe that $m_3(j\text{-}e)$ and $m_3(e\text{-}e)$ have opposite signs and that for a given N they tend to cancel each other when L increases. Indeed, for $L\gg 1$ the field $r^L Y_{L0}$ is essentially acting on the external part of the electron density. For this part, electron screening almost cancels out the jellium Coulomb potential, and, consequently, the Coulomb contribution to m_3.

The following physical picture thus emerges. For a given cluster, the excitation energy corresponding to small values of L is mainly determined by the Coulomb energy, the electron kinetic energy playing a minor role. When L increases, the Coulomb contribution becomes less important due to electron screening. Above a certain value of L, the kinetic energy is the only appreciable contribution to the surface-mode restoring force. At larger L, one expects the mode to lose its collective character: the $r^L Y_{L0}$ field will only probe the outermost single-electron contribution. Putting it in a different way, the main contribution to m_3 will come from the most external electron shell and the excitation will be of electron-hole type. Consequently, there is a critical angular momentum $L_{\rm cr}$ for the existence of collective surface modes in a given cluster N.[26]

Figure 4 shows the energies E_3 versus N for Na magic clusters of $N=8$, 20, 40, 58, 92, 138, and 198 atoms. Starting from the bottom, the curves and points correspond to $L=1$–7 and to $L=0$ (upper curve). The $L=1$–7 KS results for these clusters are represented by triangles, whereas the $L=0$ KS results are represented by crosses. The dashed lines linking the KS points are only to guide the eye. The crosses lying near the $L=1$ curve at $N=20$, 92, and 198 are the results obtained in Ref. 14, and the two crosses near the left bottom corner are the $N=8$ and 20 experimental $L=1$ values of Refs. 9 and 8, respectively. We want to stress again that E_3 is an upper bound to the resonance peak energy.

The solid lines are the TF results obtained using the kinetic-energy density (40). TF calculations are straightforward and actually we have performed them up to $N=500$. Notice that the TF results nicely average the KS ones. The main discrepancy is around $N\approx 50$ and it is due to a shell effect. Indeed, the $N=58$ cluster is obtained by adding 18 $1g$ electrons to the $N=40$ cluster. These $1g$ electrons in the more external shell contribute appreciably to the high multipolarity excitations.

$E_3(N)$ has a quite different behavior depending on the value of the angular momentum. For high L the energies decrease with N and tend to some asymptotic value. For small L the energies are rather independent of N, slightly increasing with it for small clusters. From the results shown in Tables III–V, we infer that these trends could be related to the dominance of $m_3(T)$ at high L and of $m_3(C)$ at small L (actually, for $L=1$ this is the only contribution to m_3).

To check this guess, we have resorted to a simplified model in which the electron density is taken constant up to the jellium sharp surface:

$$\rho=\rho_j=n\Theta(R-r)\ . \tag{42}$$

Then, for $L=0$, Eqs. (29) and (36) reduce to

$$\begin{aligned} m_1&=2\frac{\hbar^2}{m}4\pi n\frac{R^5}{5}\ ,\\ m_3&=2\left[\frac{\hbar^2}{m}\right]^2(4\pi n)^2e^2\frac{R^5}{5}\ . \end{aligned} \tag{43}$$

Thus

$$E_3(L=0)=\hbar\omega_p\ , \tag{44}$$

where the plasma frequency ω_p is defined as $\omega_p^2=4\pi ne^2/m$. For $L\geq 1$, using Eq. (42) and $\tau=\frac{3}{5}(3\pi^2)^{2/3}n^{5/3}\equiv\alpha n^{5/3}$, we get from Eqs. (16), (19), (26), and (28)

TABLE II. RPA $L=0$ volume mode energies E_1 and E_3 as well as m_{-1}, m_1, and m_3 sum rules (in a.u.) for several Na clusters. The different contributions to m_3 are also displayed.

N	m_{-1}	m_1	m_3	E_1	E_3	$m_3(T)$	$m_3(j\text{-}e)$	m_3(corr)
8	3.10×10^{4}	706.8	22.16	0.151	0.177	1.87	19.8	0.53
20	1.19×10^{5}	3067.0	105.9	0.161	0.186	4.86	99.7	1.35
92	1.098×10^{6}	36 980.0	1471.0	0.184	0.199	23.7	1441.0	6.28

TABLE III. RPA E_3 energies and m_1 and m_3 sum rules (in a.u.) for the $N=8$ Na cluster. The different contributions to m_3 are also displayed.

L	m_1	m_3	E_3	$m_3(T)$	$m_3(e\text{-}e)$	$m_3(j\text{-}e)$
1	0.955	1.198×10^{-2}	0.112	0.0	0.0	1.198×10^{-2}
2	1.406×10^{2}	2.240	0.126	0.743	−1.575	3.071
3	1.866×10^{4}	4.048×10^{2}	0.147	2.604×10^{2}	-3.621×10^{2}	5.066×10^{2}
4	2.690×10^{6}	8.377×10^{4}	0.176	7.006×10^{4}	-6.341×10^{4}	7.712×10^{4}
5	4.464×10^{8}	1.913×10^{7}	0.207	1.779×10^{7}	-1.089×10^{7}	1.223×10^{7}
6	8.740×10^{10}	4.794×10^{9}	0.234	4.657×10^{9}	-2.012×10^{9}	2.148×10^{9}
7	2.043×10^{13}	1.337×10^{12}	0.256	1.322×10^{12}	-4.190×10^{11}	4.334×10^{11}
8	5.737×10^{15}	4.211×10^{14}	0.271	4.195×10^{14}	-1.011×10^{14}	1.026×10^{14}
9	1.945×10^{18}	1.515×10^{17}	0.279	1.514×10^{17}	-2.868×10^{16}	2.883×10^{16}
10	8.014×10^{20}	6.265×10^{19}	0.280	6.265×10^{19}	-9.676×10^{18}	9.681×10^{18}
11	4.061×10^{23}	2.978×10^{22}	0.271	2.978×10^{22}	-3.918×10^{21}	3.912×10^{21}
12	2.550×10^{26}	1.617×10^{25}	0.252	1.617×10^{25}	-1.927×10^{24}	1.922×10^{24}
13	1.969×10^{29}	9.908×10^{27}	0.224	9.911×10^{27}	-1.165×10^{27}	1.162×10^{27}

TABLE IV. Same as Table III for $N=20$.

L	m_1	m_3	E_3	$m_3(T)$	$m_3(e\text{-}e)$	$m_3(j\text{-}e)$
1	2.387	3.150×10^{-2}	0.115	0.0	0.0	3.150×10^{-2}
2	6.100×10^{2}	9.518	0.125	1.934	−7.271	14.856
3	1.301×10^{5}	2.403×10^{3}	0.136	1.076×10^{3}	-2.947×10^{3}	4.274×10^{3}
4	2.782×10^{7}	6.489×10^{5}	0.153	4.335×10^{5}	-8.494×10^{5}	1.065×10^{6}
5	6.366×10^{9}	1.933×10^{8}	0.174	1.586×10^{8}	-2.240×10^{8}	2.587×10^{8}
6	1.613×10^{12}	6.286×10^{10}	0.197	5.719×10^{10}	-5.938×10^{10}	6.505×10^{10}
7	4.625×10^{14}	2.223×10^{13}	0.219	2.128×10^{13}	-1.665×10^{13}	1.760×10^{13}
8	1.523×10^{17}	8.601×10^{15}	0.238	8.439×10^{15}	-5.099×10^{15}	5.261×10^{15}
9	5.820×10^{19}	3.683×10^{18}	0.252	3.655×10^{18}	-1.747×10^{18}	1.775×10^{18}
10	2.597×10^{22}	1.765×10^{21}	0.261	1.760×10^{21}	-6.811×10^{20}	6.857×10^{20}
11	1.357×10^{25}	9.561×10^{23}	0.265	9.556×10^{23}	-3.058×10^{23}	3.064×10^{23}
12	8.316×10^{27}	5.905×10^{26}	0.266	5.907×10^{26}	-1.594×10^{26}	1.593×10^{26}
13	5.959×10^{30}	4.181×10^{29}	0.265	4.183×10^{29}	-9.676×10^{28}	9.658×10^{28}

TABLE V. Same as Table III for $N=92$.

L	m_1	m_3	E_3	$m_3(T)$	$m_3(e\text{-}e)$	$m_3(j\text{-}e)$
1	10.98	0.1561	0.119	0.0	0.0	0.1561
2	7.357×10^{3}	1.207×10^{2}	0.128	9.443	−92.48	2.038×10^{2}
3	3.807×10^{6}	6.726×10^{4}	0.133	1.329×10^{4}	-9.904×10^{4}	1.530×10^{5}
4	1.817×10^{9}	3.513×10^{7}	0.139	1.219×10^{7}	-7.051×10^{7}	9.344×10^{7}
5	8.499×10^{11}	1.863×10^{10}	0.148	9.414×10^{9}	-4.273×10^{10}	5.195×10^{10}
6	4.013×10^{14}	1.032×10^{13}	0.160	6.701×10^{12}	-2.409×10^{13}	2.771×10^{13}
7	1.950×10^{17}	6.010×10^{15}	0.176	4.597×10^{15}	-1.322×10^{16}	1.463×10^{16}
8	9.883×10^{19}	3.674×10^{18}	0.193	3.121×10^{18}	-7.253×10^{18}	7.805×10^{18}
9	5.287×10^{22}	2.354×10^{21}	0.211	2.137×10^{21}	-4.056×10^{21}	4.273×10^{21}
10	3.015×10^{25}	1.583×10^{24}	0.229	1.497×10^{24}	-2.347×10^{24}	2.433×10^{24}
11	1.851×10^{28}	1.121×10^{27}	0.246	1.087×10^{27}	-1.424×10^{27}	1.458×10^{27}
12	1.233×10^{31}	8.415×10^{29}	0.261	8.281×10^{29}	-9.162×10^{29}	9.296×10^{29}
13	8.996×10^{33}	6.735×10^{32}	0.274	6.684×10^{32}	-6.319×10^{32}	6.370×10^{32}

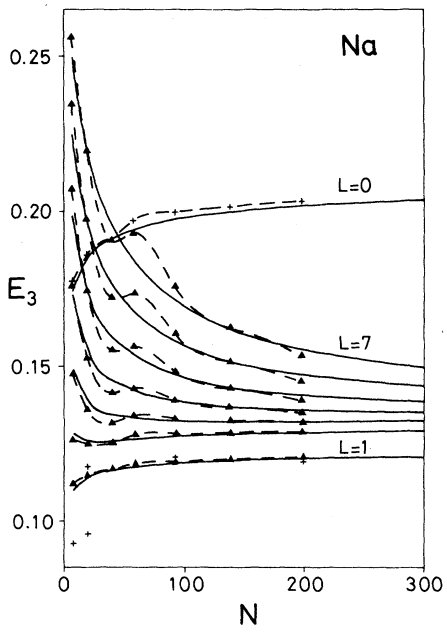

FIG. 4. E_3 energies (in a.u.) for $N=8$, 20, 40, 58, 92, 138, and 198 Na magic clusters. From bottom to top, the curves and points correspond to $L=1-7$ and $L=0$ (upper crosses and curve).

$$m_1=\frac{1}{2}\frac{\hbar^2}{m}nLR^{2L+1}\ ,$$

$$m_3=\left[\frac{\hbar^2}{m}\right]^3\tfrac{1}{3}L(2L+1)(L-1)\alpha n^{5/3}R^{2L-1}$$
$$+2\pi e^2\left[\frac{\hbar^2}{m}\right]^2 n^2R^{2L+1}\frac{L^2}{2L+1}\ . \qquad (45)$$

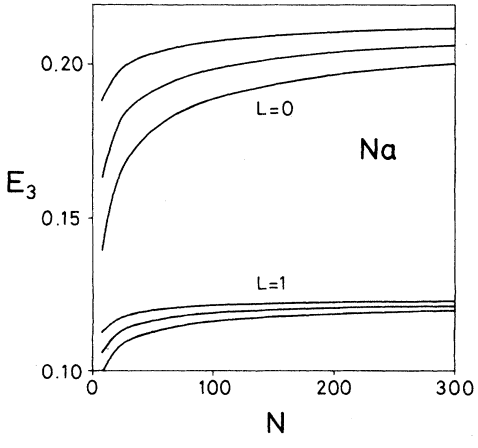

FIG. 5. $L=0$ (upper curves) and $L=1$ (lower curves) obtained in the TF approximation using Eq. (41). For each multipolarity, the curves correspond to $a=0.72$ a.u. (upper), $a=1.02$ a.u. (middle), and $a=1.32$ a.u. (lower).

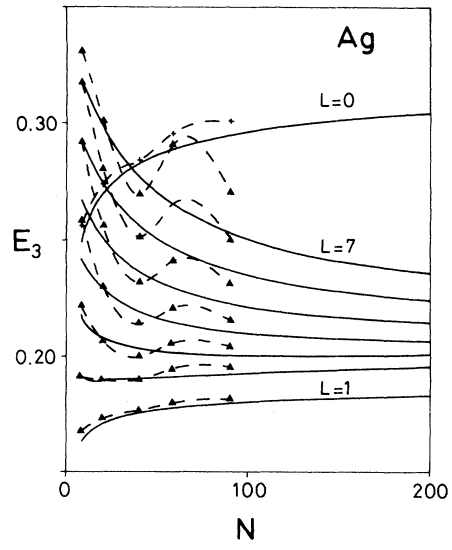

FIG. 6. Same as Fig. 4 for $N=8$, 20, 40, 58, and 90 Ag clusters.

Thus

$$E_3^2(L)=\hbar^2\omega_p^2\frac{L}{2L+1}+\tfrac{2}{3}\hbar^2(2L+1)(L-1)\frac{\beta_F^2}{R^2}\ , \qquad (46)$$

where

$$\beta_F=(\tfrac{3}{5})^{1/2}v_F=(\tfrac{3}{5})^{1/2}(3\pi^2)^{1/3}\frac{\hbar}{m}n^{1/3}\ .$$

Equations (44) and (46) explain qualitatively the behavior of $E_3(L)$ versus N. First notice that for a fixed L, when N goes to infinity we have

$$E_3^2(L)\rightarrow\hbar^2\omega_p^2\frac{L}{2L+1}\ . \qquad (47)$$

This is the classical Mie result[27] and together with Eq. (44) explains the behavior of the curves shown in Fig. 4 for big clusters.

For a given system, Eq. (46) shows that if L increases, the kinetic-energy contribution will eventually take over the Coulomb contribution. Due to the saturation condition $R=r_sN^{1/3}$, for small clusters that will happen at a value of L which is smaller than that for big clusters, explaining the $N^{-1/3}$ falloff of the $E_3(L)$ curves for $N\leq 100$ and $L\geq 4$.

The only trend this simple model cannot explain is the bending down of the E_3 curves for small N and L values. Since $m_3(L=1)$ is determined by the jellium-electron contribution, this effect might be due to the diffuseness of the electron density, which has not been considered in Eq. (42). To confirm this possibility, we have artificially changed the diffuseness parameter a entering Eq. (41) and

computed the $L=0$ and $L=1$ modes for Na clusters.

Figure 5 shows the results we have obtained using different values of a. For each multipolarity, the upper curve corresponds to $a=0.72$, the middle curve to $a=1.02$ (fit value), and the lower curve to $a=1.32$ a.u. We see from this figure that the bending down increases when a increases. Besides the bending, increasing the surface diffuseness also causes a global shift of the E_3 curves downwards. Thus, we conclude that the red shifting of the dipole mode from the classical Mie value is a surface-diffuseness effect.

We have also verified that the Na adjusted density (41) reproduces the TF results fairly well up to $L\approx 4$. Above this value, it fails for clusters $N\leq 40$, but still yields good results for bigger L, provided $N>40$.

Figure 6 collects the E_3 energies for silver. The triangles represent the magic Ag clusters $N=8$, 20, 40, 58, and 90 results. As in Fig. 4, the dashed lines have been drawn only to guide the eye. The solid lines are the TF energies. From bottom to top, the curves and points correspond to $L=1-7$ and to $L=0$. We see that in this case the TF results do not average the KS ones. Had we used for Ag a smaller value of β (≈ 0.5), the agreement between TF and KS would have been much better.

Qualitatively, Figs. 4 and 6 look very much the same. In the case of Ag the shell effect from $N=40$ to 58 is also quite distinct. The bending down of the $L=1$ mode is more pronounced for Ag than Na. This is so because the diffuseness corrections to the bulk E_3, Eq. (46), are of order $(a/r_0N^{1/3})^2$ and consequently bigger for Ag than for Na. The density (41) with the parameters corresponding to Ag can be used for a quick estimate of E_3, with the same remarks as in the Na case.

Finally, we can use Eq. (46) to estimate a lower bound of the critical angular momentum $L_{\rm cr}$ discussed at the beginning of this section. We have argued that the mode will not lose its collective character until the kinetic dominates over the Coulomb contribution to m_3. Imposing that both contributions be the same,

$$\hbar^2\omega_p^2\frac{L}{2L+1}=\tfrac{2}{3}\hbar^2(2L+1)(L-1)\frac{\beta_F^2}{R^2}\ .$$

For high L values, it yields

$$L_{\rm cr}>L\approx\sqrt{3/8}\frac{\omega_p}{\beta_F}r_sN^{1/3}\approx 0.7r_s^{1/2}N^{1/3}\ . \tag{48}$$

This *lower bound* $L_{\rm cr}$ is similar to the one obtained by Ekardt,[26] who arrives at the same expression with 0.9 instead of 0.7.

V. DISCUSSION AND CONCLUDING REMARKS

In this paper we have studied the surface modes of clusters and spheres of metal atoms within the RPA sum-rule approach. We have obtained *with RPA precision* the m_1 and m_3 moments of the strength function for operators of the kind r^LY_{L0}. This allows us to define an average energy which, neglecting electron kinetic-energy contributions and surface-diffuseness corrections, reduces to the classical Mie formula when N goes to infinity.

The expressions we have deduced are very simple to use and could be applied to other metals besides the ones we have studied here. The key ingredients for computing m_1 and m_3 are the *ground-state* kinetic and particle electron densities which can be easily obtained from a spherical Kohn-Sham calculation. In this way, we are introducing a realistic electron-density profile. The importance of surface inhomogeneities on the dispersion of surface modes, i.e., the dependence of a surface-mode frequency upon the radius and surface diffuseness of the sphere, was stressed in Ref. 3 (see also Ref. 5).

This dispersion comes out from our model in a very natural way. For $L>1$ we have an R (N) dependence from quantum-size effects associated with the electron kinetic energy [Eq. (46)]; the surface-diffuseness effect is far less important, at least for small clusters and angular momenta. On the contrary, electron surface diffuseness is the only dispersion source for the dipole mode.

We have found that shell effects are important only in cases where high-angular-momentum electron orbits are involved. Thus, a semiclassical TF calculation gives results that agree well with the KS ones, provided an effective Weizsäcker correction to the TF kinetic-energy density is included.

The present method is of great simplicity and usefulness. It can be readily used to obtain E_3 collective energies with RPA precision, or just the average trend by using a semiclassical model like TF. Moreover, the expression for $E_3(L)$ is simple enough to allow for a qualitative analysis of it as a function of the number of atoms N. For small values of L, we have stressed the important role played by the electron-density diffuseness to red shift the collective energies from the classical Mie value. The role played by the electron-density surface diffuseness on the dynamical polarizability of surface modes was already pointed out by Ekardt.[12]

For $L\geq 3$ the increasing contribution of the electron kinetic energy to E_3 completely changes the picture and we may have a sizable blue shifting of the collective energy for $N\leq 100$. It is worth mentioning that recent experiments performed on Ag spheres of 40–70 nm have been reported,[6] confirming the validity of the Mie model to study $L=1$ and 2 optical-absorption spectra. Our analysis shows that no deviations from the Mie model should be expected for these Ag spheres and L modes. In order to observe a significant deviation from this model, one should appreciably excite $L\geq 3$ modes on much smaller spheres. However, for such spheres retardation effects might be large.[6]

The interplay between Coulomb and kinetic contributions to E_3 can be used to determine roughly at which angular momentum the modes are no longer collective. We have argued that this could only happen after the kinetic contribution takes over the Coulomb contribution. Using this simple argument, we have found a value for $L_{\rm cr}$ that agrees well with previous estimates by Ekardt.

Finally, we have also discussed the $L=0$ volume mode calculating with RPA precision the m_{-1}, m_1, and m_3 moments of the strength function. We have shown that

there is some collectivity concentrated in this mode, which lies at much higher energy than the surface modes which we have thoroughly studied.

During the completion of this work, we became aware of a calculation by Brack,[28] who arrived at the same expressions for m_3 using a similar technique. However, for the numerical applications he used a trial density TF method instead of the quantal KS and only discussed Na clusters. In this sense, we consider both calculations as complementary.

ACKNOWLEDGMENTS

We are indebted to Nuria Barberán and Montserrat Casas for many useful discussions and to Julio Alonso and Pilar Iñiguez for their interest in this study. This work has been supported in part by the Comisión Asesora de Investigación Científica y Técnica (CAICyT), Spain, under Grant No. PB85-0072-C02-00, and by the University of Valencia–University of the Balearic Islands exchange program.

[1]M. A. Smithard, Solid State Commun. **13**, 153 (1973).
[2]J. D. Ganière, R. Rechsteiner, and M. A. Smithard, Solid State Commun. **16**, 113 (1975).
[3]A. D. Boardman and B. U. Paranjape, J. Phys. F **7**, 1935 (1977).
[4]P. E. Batson, Phys. Rev. Lett. **49**, 986 (1982).
[5]N. Barberán and M. Batlle, J. Phys. C **20**, 3583 (1987).
[6]B. K. Russell, J. G. Mantovani, V. E. Anderson, R. J. Warmack, and T. L. Ferrell, Phys. Rev. B **35**, 2151 (1987).
[7]R. Rojas, F. Claro, and R. Fuchs, Phys. Rev. B **37**, 6799 (1988).
[8]W. A. de Heer, K. Selby, V. Kresin, J. Masui, M. Vollmer, A. Châtelain, and W. D. Knight, Phys. Rev. Lett. **59**, 1805 (1987).
[9]K. Selby, M. Vollmer, J. Masui, V. Kresin, M. Kruger, W. A. de Heer, and W. D. Knight (unpublished).
[10]W. D. Knight, K. Clemenger, W. A. de Heer, and W. A. Saunders, Phys. Rev. B **31**, 2539 (1985).
[11]M. J. Stott and E. Zaremba, Phys. Rev. A **21**, 12 (1980).
[12]W. Ekardt, Phys. Rev. Lett. **52**, 1925 (1984).
[13]W. Ekardt, Phys. Rev. B **31**, 6360 (1985).
[14]G. Bertsch and W. Ekardt, Phys. Rev. B **32**, 7659 (1985).
[15]O. Bohigas, A. M. Lane, and J. Martorell, Phys. Rep. **51**, 267 (1979).
[16]S. Stringari, Ann. Phys. (N.Y.) **151**, 35 (1983); E. Lipparini and S. Stringari, Phys. Rep. **175**, 103 (1989).
[17]M. Barranco, A. Polls, and J. Martorell, Nucl. Phys. A **444**, 445 (1985).
[18]E. Suraud, M. Barranco, and J. Treiner, Nucl. Phys. A **480**, 29 (1988).
[19]M. Casas and J. Martorell, Nucl. Phys. A **490**, 329 (1988).
[20]N. D. Lang and W. Kohn, Phys. Rev. B **1**, 4555 (1970).
[21]Ll. Serra, Master's thesis, University of Baleares, Mallorca, Spain, 1988.
[22]M. Y. Chow, A. Cleland, and M. L. Cohen, Solid State Commun. **52**, 645 (1984).
[23]M. P. Iñiguez, J. A. Alonso, and L. C. Balbás, Solid State Commun. **57**, 85 (1986).
[24]M. P. Iñiguez, C. Baladrón, and J. A. Alonso, Surf. Sci. **127**, 367 (1983).
[25]Nguyen Van Giai, Phys. Lett. **105B**, 11 (1981).
[26]W. Ekardt, Phys. Rev. B **32**, 1961 (1985).
[27]G. Mie, Ann. Phys. **25**, 377 (1908).
[28]M. Brack, Phys. Rev. B (to be published).